Colloids and Surfaces A: Physicochemical and Engineering Aspects 742 (2026) 140411

Contents lists available at ScienceDirect

Colloids and Surfaces A: Physicochemical and Engineering Aspects

journal homepage: www.elsevier.com/locate/colsurfa

Defect-enhanced interfacial interaction in Co_2B/Fe_2O_3 heterostructures boosts hydrogen generation from $NaBH_4$ hydrolysis

Huaxia Zhou [a], Shuyi Shang [a], Boxuan Lu [a], Tayirjan Taylor Isimjan [b,*], Xiulin Yang [a,*]

[a] Guangxi Key Laboratory of Low Carbon Energy Materials, School of Chemistry and Pharmaceutical Sciences, Guangxi Normal University, Guilin 541004, China
[b] Saudi Arabia Basic Industries Corporation (SABIC) at King Abdullah University of Science and Technology (KAUST), Thuwal 23955-6900, Saudi Arabia

HIGHLIGHTS

- Co_2B/Fe_2O_3-CNTs heterojunction was synthesized via a multi-step synthesis.
- It shows high HGR (5227.07 mL min^{-1} g_{cat}^{-1}) and excellent reusability.
- CNTs support enables effective dispersion of active components.
- Heterojunction structure regulates electron density at active sites.

GRAPHICAL ABSTRACT

A Co_2B/Fe_2O_3-CNTs heterojunction catalyst was synthesized, exhibiting an exceptional hydrogen generation rate (5227.02 mL min^{-1} g_{cat}^{-1}). This performance stems from the CNTs-enabled dispersion of active components, a heterojunction architecture that shortens ion diffusion pathways, and synergistic electron modulation at the active sites.

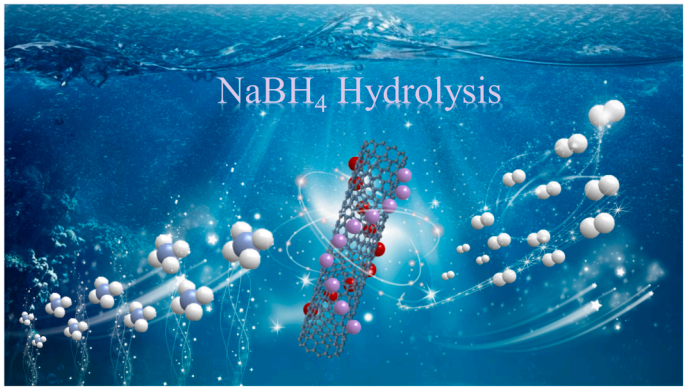

ARTICLE INFO

Keywords:
Co_2B/Fe_2O_3-CNTs
Carbon nanotubes
Heterojunctions
Electronic synergy
$NaBH_4$ hydrolysis

ABSTRACT

Designing a cost-effective, high-performance catalyst for $NaBH_4$ hydrolysis represents a key step toward developing sustainable hydrogen sources. In this study, a Co_2B/Fe_2O_3 heterojunction catalyst supported on CNTs was successfully synthesized via a combined hydrothermal, pyrolysis, and chemical-reduction strategy. Structural characterization confirmed the successful formation of Co_2B and Fe_2O_3 phases anchored on CNTs, forming well-defined nanoscale interfaces with abundant lattice defects and uniform elemental dispersion. X-ray photoelectron spectroscopy revealed strong interfacial electronic coupling, in which some electrons are transferred to adjacent sites across the heterojunction interface between Co_2B and Fe_2O_3, forming an electron gradient, modulating the local charge density, and enhancing catalytic activity. The optimized Co_2B/Fe_2O_3-CNTs catalyst exhibited an exceptional hydrogen generation rate (HGR) of 5227.02 mL min^{-1} g_{cat}^{-1}. Studies found that the higher charge attraction properties (−16.81 mV) and favorable hydrophilicity (21.2) endow the Co_2B/Fe_2O_3-CNTs catalyst with a strong adsorption capacity for negatively charged BH_4^-. The catalyst retained ~70% of its initial activity after five cycles, demonstrating good reusability and structural stability. A mechanistic study based on the

* Corresponding authors.
E-mail addresses: isimjant@sabic.com (T.T. Isimjan), xlyang@gxnu.edu.cn (X. Yang).

https://doi.org/10.1016/j.colsurfa.2026.140411
Received 8 January 2026; Received in revised form 13 March 2026; Accepted 30 March 2026
Available online 1 April 2026

Michaelis–Menten model indicates that BH_4^- species are activated at Co_2B sites, while H_2O molecules are dissociated at Fe_2O_3 sites, synergistically promoting H-H bond formation and efficient hydrogen release. The Co_2B/Fe_2O_3-CNTs catalyst thus provides a cost-effective, magnetically separable, and reusable platform for sustainable on-demand hydrogen generation.

1. Introduction

Against the backdrop of increasing non-renewable energy consumption and worsening environmental pollution, hydrogen has emerged as an ideal energy carrier due to its high energy density and environmentally benign characteristics [1–3]. Sodium borohydride ($NaBH_4$), with a high hydrogen content of 10.8 wt%, exhibits excellent stability in alkaline solutions and generates environmentally friendly, recyclable byproducts, making it a promising candidate for chemical hydrogen storage [4]. Hydrogen production from sodium borohydride exhibits exceptional versatility. It not only serves as an efficient hydrogen source for the clean energy sector, but also plays a critical role in healthcare applications and organic chemical synthesis. The catalytic hydrolysis of $NaBH_4$ enables controllable hydrogen release with rapid reaction kinetics. However, challenges such as slow self-hydrolysis rates and suboptimal hydrogen yield efficiency remain unresolved, underscoring the need for highly efficient catalysts. Although noble metal catalysts such as ruthenium [5], platinum [6], and palladium [7], exhibit superior catalytic performance, their widespread use is limited by high cost, resource scarcity, and complex recovery processes. This has prompted extensive research into non-noble metal alternatives [8]. Among these, cobalt-based catalysts have attracted considerable attention owing to their high catalytic activity, facile synthesis, and favorable cost-effectiveness [9]. Nevertheless, thermal effects during the reaction can induce particle agglomeration, thereby reduce active sites and diminish catalytic efficiency [10–13]. To mitigate this issue, researchers have enhanced the dispersion and catalytic performance of cobalt-based catalysts by employing supports with high specific surface areas and favorable electronic properties, such as nickel foam [14] and three-dimensional graphene oxide [10]. Notably, integrating cobalt-based catalysts with sustainable and stable carbon supports, such as carbon nanotubes (CNTs) [15], graphene [16], and biomass-derived carbon [17], effectively suppresses nanoparticle aggregation and enhances overall catalytic activity [18]. For example, Katabathini et al. [15] synthesized cobalt oxide supported on multi-walled carbon nanotubes (Co/MWCNTs) using an impregnation method. Experimental results showed that at 35°C, the hydrogen evolution rate of the Co/MWCNTs-20 catalyst reached 409 mL min^{-1} g_{cat}^{-1}, compared to only 28 mL min^{-1} g_{cat}^{-1} for the bare MWCNTs support. This remarkable improvement was attributed to the large surface area provided by the MWCNTs and the enhanced dispersion of the active metallic phase.

Efforts to enhance the hydrolysis activity of sodium borohydride have focused on various strategies, including designing novel material structures [19], optimizing synthesis methods [20], constructing composites [21], doping [22], introducing defects and vacancies [23]. Among these approaches , transition metal-based hetero-structural materials are a class of very promising substitutes for noble metal-based catalysts for high-performance catalysis, due to their inherent internal electric field at the interface in the heterojunctions, which could induce electron re-localization and facilitate charge carrier migration between different metal sites at hetero-structural boundaries [24]. By leveraging these properties, combining cobalt-based catalysts with metal oxide-modified carbon nanotubes to form composite heterojunction materials demonstrates significant potential in the $NaBH_4$ hydrolysis [25,26]. Moreover, defect engineering represents an effective strategy for enhancing catalytic activity. By precisely tuning the electronic structure and carrier concentration of the catalyst, engineered defects enable fine control over catalytic performance [27,28]. The feasibility of this approach has been demonstrated in our previous work, where boron and oxygen vacancy catalysts exhibited high efficiency for $NaBH_4$ hydrolysis [29,30]. Further investigations reveal that lattice expansion through heteroatom doping not only provides additional space for reactant accommodation but also enhances the electrical conductivity of the catalyst, thereby improving charge transport efficiency and reaction kinetics [31].

Building on these insights, the present study successfully synthesized a heterojunction catalyst, Co_2B/Fe_2O_3, supported on CNTs using a defect engineering approach. Characterization results reveal that employing CNTs as a support enhances particle dispersion, thereby increasing the number of accessible active sites. Simultaneously, the heterojunction formed between Co_2B, Fe_2O_3, and CNTs exposes a larger portion of the layered pore framework on the surface, creating shorter pathways for ion diffusion and accelerating mass transport. These heterointerfaces exhibit modified electronic structures that promote rapid electron transfer. Performance evaluation demonstrated that the Co_2B/Fe_2O_3-CNTs catalyst exhibits outstanding hydrogen generation capability, achieving a hydrogen generation rate (HGR) of 5227.02 mL min^{-1} g_{cat}^{-1}. The exceptional catalytic activity stems from strong electronic interactions between the Fe, Co and B, which enhance the dissociation and adsorption of H_2O molecules and BH_4^- ions, thereby promoting the catalytic hydrolysis of $NaBH_4$ and enabling highly efficient hydrogen production.

2. Experimental section

2.1. Materials

Iron acetylacetonate ($Fe(C_5H_7O_2)_3$, ≥ 98%, Aladdin), cobalt chloride hexahydrate ($CoCl_2{\cdot}6\,H_2O$, ≥ 99.0%, Aladdin), carbon nanotubes (CNTs, ≥ 99.0%, Aladdin), urea (H_2NCONH_2, ≥ 99.0%, Aladdin), sodium borohydride ($NaBH_4$, ≥ 98.0%, Sinopharm), sodium hydroxide (NaOH, ≥ 96.0%, Aladdin), and anhydrous ethanol (C_2H_6O, ≥ 99.7%, Xilong Scientific). All reagents were commercially available and used as received without further purification. All aqueous solutions were prepared using deionized water.

2.2. Synthesis of Fe_2O_3-CNTs

Carbon nanotubes (0.5 g) and iron acetylacetonate (2.0 g) were dispersed in 100 mL of anhydrous ethanol and subjected to ultrasonication for 15 min. Subsequently, 20 mL of 6 M NaOH solution and 60 mL of ethanol were added to the mixture. The resulting suspension was transferred to a sealed reactor and heated at 200 °C for 2 h. After cooling to room temperature, the product was collected by centrifugation, thoroughly washed with deionized water and ethanol, and dried overnight. The obtained solid was then calcined at 500 °C under a nitrogen atmosphere at a heating rate of 10 °C/min for 2 h, yielding the Fe_2O_3-CNTs composite.

2.3. Synthesis of Co_2B/Fe_2O_3-CNTs

During the synthesis process, a specified amount of Fe_2O_3-CNTs was dispersed in a beaker containing $CoCl_2{\cdot}6\,H_2O$. An appropriate amount of water was added, followed by ultrasonic treatment for 30 min and stirring at 600 r min^{-1} for 1 h, after which the solvent was evaporated. In a mortar, mix the dried sample with 0.8 g of urea and grind manually. Then add 4 mmol of $NaBH_4$ and disperse it uniformly in the mortar. Grind by hand until the mixture turns black. Transfer the mixture to a

beaker, add an appropriate amount of deionized water, centrifuge, and wash three times with water and ethanol. followed by vacuum drying at 60 °C for 12 h. Single Co_2B and Co_2B-CNTs were prepared without Fe_2O_3-CNTs or Fe_2O_3.

3. Results and discussion

3.1. Synthesis strategy and microstructural analysis

The synthesis of Co_2B/Fe_2O_3-CNTs heterojunction materials was carried out via a combined process comprising hydrothermal treatment, pyrolysis, and chemical reduction. As illustrated in Fig. 1a, the synthetic procedure proceeds as follows: First, the Fe^{3+}-CNTs intermediate is prepared via a hydrothermal method. This intermediate is subsequently calcined at 500 °C for 2 h under a nitrogen atmosphere to yield the Fe_2O_3-CNTs composite. The formation of Fe_2O_3 is confirmed by X-ray diffraction (XRD) analysis in Fig. 1b, which shows characteristic diffraction peaks corresponding to hematite (JCPDS: 39–1346) [32]. In the next step, the Fe_2O_3-CNTs composite is dispersed uniformly in ethanol via ultrasonication. $CoCl_2{\cdot}6\,H_2O$ is then introduced into the suspension, followed by thorough mixing and solvent removal via vacuum evaporation, resulting in the formation of the Co^{2+}/Fe_2O_3-CNTs precursor. This precursor is mixed with urea in a mortar and ground manually to ensure homogeneity. Subsequently, $NaBH_4$ is added to initiate a chemical reduction reaction, ultimately yielding the $Co_2B/$-Fe_2O_3-CNTs heterojunction catalyst. XRD analysis in Fig. 1b reveals a broad peak centered at approximately 26.4°, attributed to the (002) plane of graphitic carbon [33]. After reduction with $NaBH_4$, weak diffraction peaks appear at around 35.74° and 45.72°, corresponding to the (220) and (211) planes of Co_2B (JCPDS: 25–0241), respectively. The low intensity and broad nature of these peaks suggest that the Co_2B nanoparticles are nanoscale in size and exhibit low crystallinity [34]. Meanwhile, the characteristic peaks of Fe_2O_3 remain clearly visible at approximately 35.63° and 43.28°, corresponding to the (311) and (400) crystallographic planes, respectively, confirming the structural integrity of the support after modification. These results confirm the successful deposition of Co_2B on the Fe_2O_3-CNTs substrate and the formation of a heterojunction structure, as further corroborated by high-resolution transmission electron microscopy (HR-TEM) analysis. XRD characterization was also performed on the reference samples. Fig. S1a confirms the phase purity of the as-used CNTs (JCPDS: 41–1487), while Fig. S1b further verifies that the cobalt-containing species deposited on the Fe_2O_3-CNTs composite is Co_2B (JCPDS: 25–0241). Electron paramagnetic resonance (EPR) spectroscopy was employed to assess defect concentration and electronic states, given its high sensitivity to unpaired electrons. The EPR signal at $g = 2.16$ in Fig. 1c indicates the successful incorporation of cobalt-related defects into the material. This may be attributed to the differing crystal structures of Co_2B and Fe_2O_3, which result in a lattice mismatch during loading [35]. This mismatch will cause lattice distortion at the interface and in the surrounding areas, as well as damage to the regularity of the atomic arrangement, which will lower the overall crystallinity and produce many lattice defects [36]. Notably, Fe_2O_3-CNTs did not exhibit this characteristic. With the incorporation of cobalt, the abundant cobalt vacancies and associated unpaired electrons in the Co_2B/Fe_2O_3-CNTs system significantly modulated the local electronic structure and orbital coupling. This exposed more active sites, thereby optimizing the adsorption capacity of active intermediates [37]. Simultaneously, the increase of defects can change the carrier concentration of the catalyst and enhance the synergistic effect of the components, thereby enhancing catalytic performance [38]. Collectively, the elevated defect density in Co_2B/Fe_2O_3-CNTs modifies the electronic structure, modulates charge carrier concentration, enhances interfacial synergy among components, and provides abundant active sites for adsorption, thereby significantly improving catalytic activity [39]. To further investigate the interfacial properties, zeta potential measurements were conducted. As illustrated in Fig. 1d, the incorporation of CNTs substantially enhanced the negative charge density of the catalyst relative to Co_2B. This improvement is attributed to an increased specific surface area and enhanced porosity, which facilitate more efficient negative charge transfer. The zeta potential of Co_2B/Fe_2O_3-CNTs is

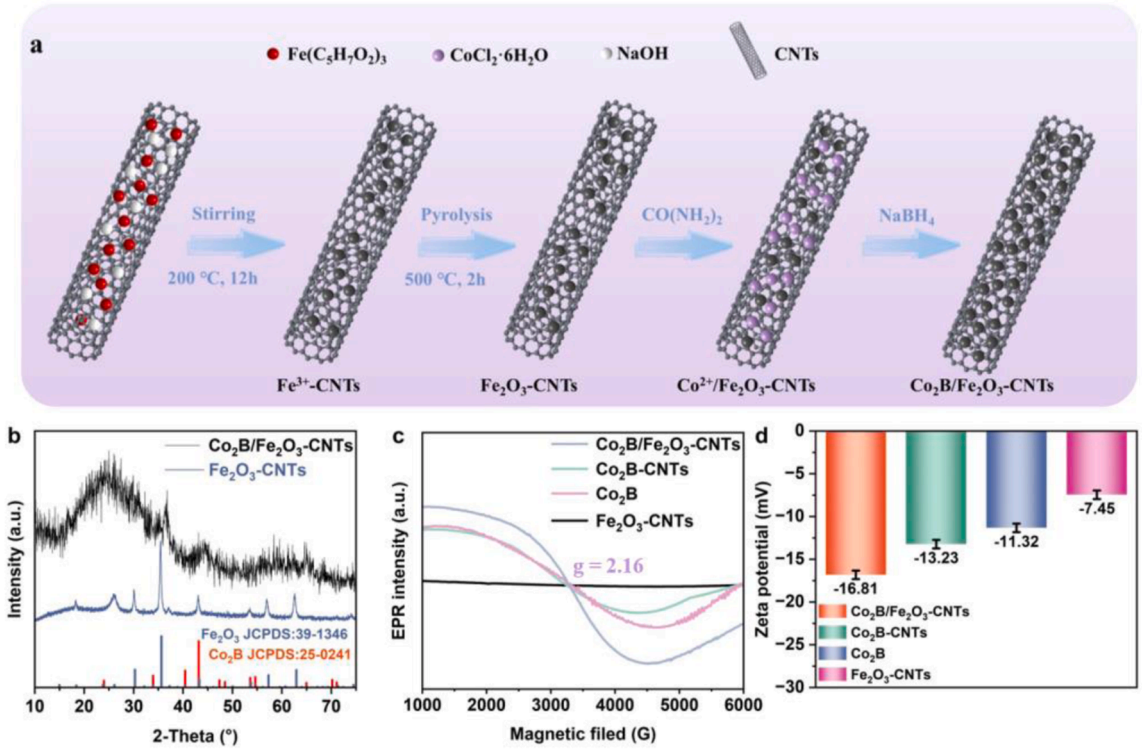

Fig. 1. (a) Schematic protocol of the synthesis strategy for Co_2B/Fe_2O_3-CNTs. (b) XRD pattern of Fe_2O_3-CNTs and Co_2B/Fe_2O_3-CNTs. (c) EPR spectra of different catalysts. (d) Zeta potential of different catalysts in $NaBH_4$ solution.

−16.81 eV, notably lower than that of Fe_2O_3-CNTs (−7.45 eV), Co_2B-CNTs (−13.23 eV) and Co_2B (−11.32 eV), indicating a higher density of surface negative charges. This characteristic strengthens electrostatic attraction toward positively charged species and promotes favorable interactions with negatively charged reactants, thereby enhancing adsorption and accelerating the hydrolysis reaction [40].

Scanning electron microscopy (SEM) and transmission electron microscopy (TEM) were employed to investigate the microstructure of Co_2B/Fe_2O_3-CNTs composites. As shown in Fig. 2Sa, Fe_2O_3-CNTs exhibit a filamentous morphology, with Fe_2O_3 nanoparticles anchored on the outer surface of carbon nanotubes. Upon incorporation of the cobalt-based component, the CNTs retain a fibrous architecture and are uniformly dispersed among the Co_2B nanoparticles (Fig. 2a). In Fig. S2b, pure Co_2B displays a distinctly nanostructured morphology. While this increases surface area, it is accompanied by significant particle agglomeration, which may impede catalytic activity. In contrast, Co_2B/Fe_2O_3-CNTs exhibit nanoscale granular morphologies with relatively uniform particle distributions, indicating superior suitability for catalytic applications. Notably, the presence of carbon nanotubes effectively mitigates agglomeration observed in pure Co_2B, thereby enhancing the dispersion of active components. This improved dispersion likely increases the accessible active surface area, a critical factor in boosting catalytic efficiency. Transmission electron microscopy (TEM) analysis further corroborates the morphological characteristics. The TEM image of Co_2B/Fe_2O_3-CNTs (Fig. 2b) reveals distinct grain boundaries, confirming its composition of intertwined fibrous carbon nanotubes and discrete nanoparticles. Moreover, a straightforward interface is observed between Co_2B and Fe_2O_3 (Fig. 2c). High-resolution TEM images show well-resolved lattice fringes with interplanar spacings of 0.215 nm and 0.237 nm, corresponding to the (211) plane of Co_2B and the (400) plane of Fe_2O_3, respectively. These results indicate that the heterojunction structure contains numerous densely packed interfaces, which facilitate efficient electron transfer across the phases [41]. Elemental mapping of Co_2B/Fe_2O_3-CNTs confirms the homogeneous distribution of Co, Fe, B, and O elements throughout the material (Figs. 2d-2h), further supporting the formation of a well-integrated heterostructure. Collectively, the designed heterostructure enables strong interfacial synergy, overcoming the inherent limitations of single-component catalysts. Furthermore, the use of carbon nanotubes as a support enhances nanoparticle dispersion and structural stability, thereby improving the performance of sodium borohydride hydrolysis. Contact angle measurements evaluated the catalyst's hydrophilic nature. The Co_2B/Fe_2O_3-CNTs composite exhibits a contact angle of 21.2°, significantly lower than those of Fe_2O_3-CNTs (55.1°), and pure Co_2B (27.8°), demonstrating superior hydrophilicity (Figs. 2i-2k). This reduced contact angle reflects enhanced interfacial water adsorption on the catalyst surface, facilitating reactant accessibility and improving catalytic activity [42].

The actual structures and elemental chemical states of Co_2B/Fe_2O_3-CNTs and Co_2B were investigated using X-ray photoelectron spectroscopy (XPS). The full XPS survey spectrum of Co_2B/Fe_2O_3-CNTs confirms the presence of Co, Fe, B, and O elements (Fig. S3). In the high-resolution C 1*s* spectra of both Co_2B/Fe_2O_3-CNTs and Co_2B, four characteristic peaks are observed: a C═C peak at 284.0 eV, a C–C peak at 284.80 eV, a C–O peak at 286.0 eV, and a C═O peak at 288.88 eV (Fig. S4a and Fig. S4b). All core-level spectra were calibrated with reference to the C 1*s* binding energy at 284.80 eV as an internal standard [43]. For the Co 2*p* spectrum (Fig. 3a), the peaks at 777.22/777.12 eV, 780.53/780.30 eV, 782.15/782.10 eV, 785.26/785.26 eV are assigned to Co–B, Co^{3+}, Co^{2+}, and satellite peaks, respectively [44,45]. The

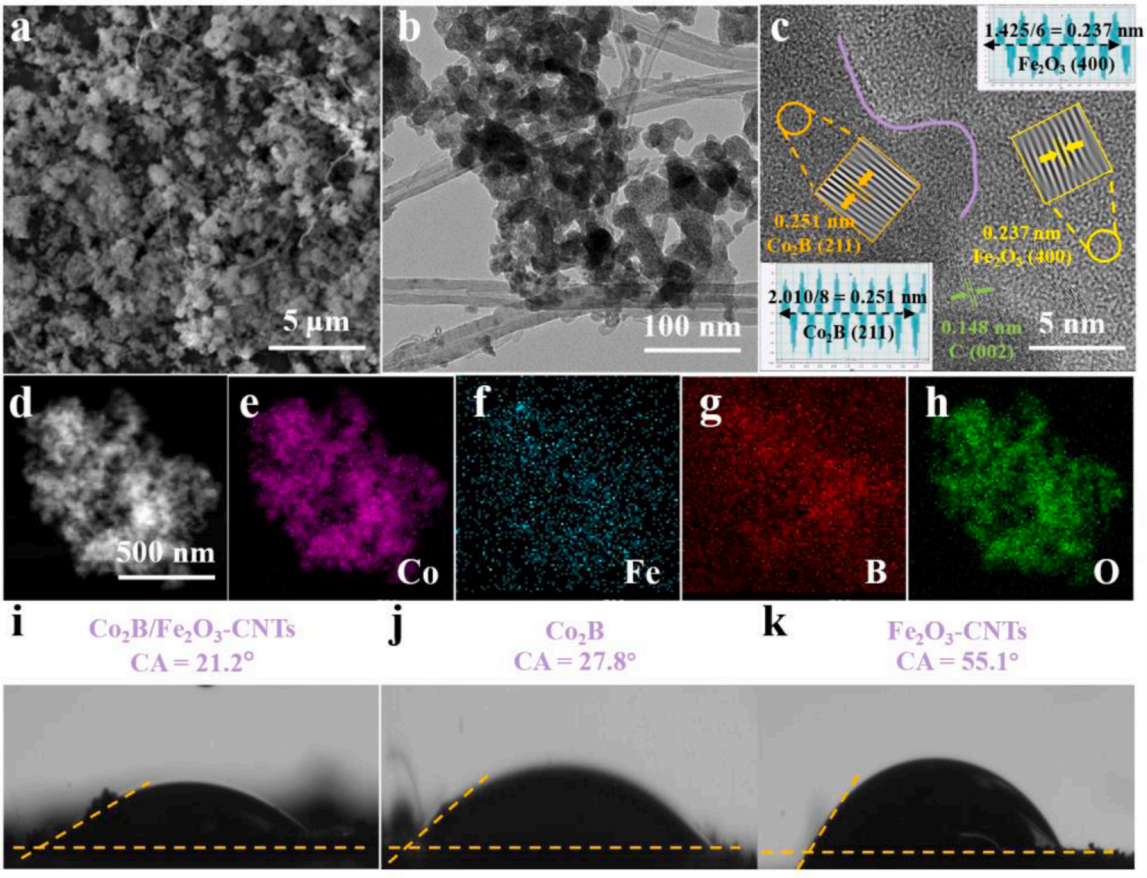

Fig. 2. (a) SEM image of the Co_2B/Fe_2O_3-CNTs. (b) TEM and (c) high-resolution TEM (HR-TEM) images of the Co_2B/Fe_2O_3-CNTs. (d-h) HAADF-STEM image and the corresponding elemental mappings (Co, Fe, B, and O) of the Co_2B/Fe_2O_3-CNTs. (i-k) Contact angle measurement of different catalysts.

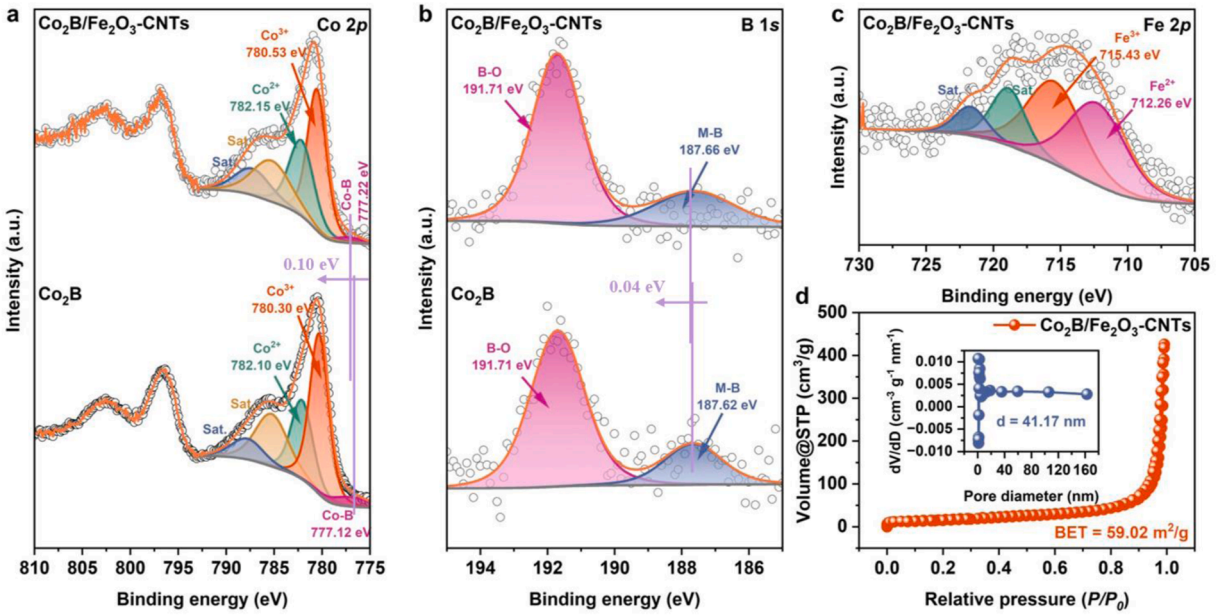

Fig. 3. High-resolution XPS spectra of Co_2B/Fe_2O_3-CNTs, and Co_2B-CNTs for (a) Co 2*p*, (b) B 1*s*, and (c) Fe 2*p*. (d) N_2 adsorption-desorption isotherms, with insets showing the corresponding pore size distributions of Co_2B/Fe_2O_3-CNTs.

presence of Co^{3+} in Co_2B is because Co^{2+} is inevitably oxidized to Co^{3+} during the synthesis process [46,47]. Deconvolution of the B 1*s* core-level spectra for both Co_2B/Fe_2O_3-CNTs reveals two distinct components corresponding to M–B (187.66 eV) (M = Co, Fe) bonds and B–O (191.71 eV) bonds, confirming the formation of a metal-boron alloy phase (Fig. 3b) [48]. The M–B peak was shifted positively by approximately 0.66 eV compared to elemental B (187.00 eV). This shift suggests electron transfer from alloyed B to the vacant d-orbitals of metallic Co and Fe, resulting in electron deficiency at B and electron enrichment at Co/Fe [49,50]. These findings highlight the strong interactions between the Co_2B and Fe_2O_3 components within the catalyst. These interactions lead to variations in electron cloud densities, which enhance charge carrier transport and significantly improve the overall catalytic performance. Furthermore, the high-resolution Fe 2*p* spectrum of Co_2B/Fe_2O_3-CNTs was deconvoluted into four components: Fe^{2+} (712.26 eV), Fe^{3+} (715.43 eV), and two satellite peaks (Fig. 3c) [51–53]. In summary , the outer electrons are difficult to stably combine at the interface of the heterostructure, resulting in some electrons being transferred to adjacent positions through the heterojunction interface between Co_2B and Fe_2O_3, forming an electron gradient. It promoted directional migration of charges from low- to high-electronegativity sites [54]. This difference in crystal and electronic structure between the two results in a unique interfacial coupling effect [55,56]. Therefore, compared with Co_2B, Co_2B/Fe_2O_3-CNTs shows better catalytic activity. N_2 adsorption-desorption isotherms show that Co_2B/Fe_2O_3-CNTs exhibits a specific surface area of 59.02 $m^2 \cdot g^{-1}$ and an average pore diameter of 41.17 nm, indicative of a typical porous heterogeneous architecture (Fig. 3d). Compared to the reference samples Co_2B and Fe_2O_3-CNTs, the Co_2B/Fe_2O_3-CNTs composite displays an increased specific surface area and enlarged pore size (Fig. S5a and Fig.S5b). This enhanced textural property provides a greater number of accessible active sites, facilitates charge carrier diffusion and mass transport, and optimizes diffusion pathways for reactants and products [57–59]. These structural and electronic synergies collectively contribute to significantly improved catalytic efficiency in the hydrolysis of sodium borohydride [60].

3.2. Catalytic activity

The catalytic performance was evaluated at 25 °C using a 150 mM $NaBH_4$ solution containing 0.4 wt% NaOH to maintain alkaline stability. The schematic illustration of the experimental setup is provided in Fig. S6. In the absence of a catalyst, weak self-hydrolysis was observed in the 150 mM $NaBH_4$ aqueous solution (Fig. S7a), whereas negligible self-hydrolysis occurred in the same solution supplemented with 0.4 wt% NaOH (Fig. S7b), confirming the stabilizing effect of alkaline conditions on $NaBH_4$. The catalytic activities of different materials—Co_2B/Fe_2O_3-CNTs, Co_2B-CNTs, Fe_2O_3-CNTs, Co_2B, and CNTs—were systematically compared in terms of $NaBH_4$ hydrolysis performance. Among them, the Co_2B/Fe_2O_3-CNTs catalyst exhibited the fastest reaction kinetics, achieving a hydrogen production rate of 5227.02 mL min^{-1} g_{cat}^{-1}, significantly surpassing all other tested catalysts (Fig. 4a and Fig. 4b). Compared to Co_2B-CNTs, the incorporation of a small amount of Fe into the Co_2B/Fe_2O_3-CNTs composite enhances electron enrichment at Co active sites, strengthens BH_4^- adsorption, and thereby improves the intrinsic catalytic activity of cobalt [61]. This result highlights the synergistic electronic interaction and the presence of highly active interfacial sites between Co and Fe in the heterostructure [62]. Compared to Co_2B, the incorporation of CNTs significantly enhances the catalyst's catalytic activity, primarily due to the increased surface area, which provides more active sites. Simultaneously, the Fe_2O_3-CNTs composite, with more active sites and a larger surface adsorption capacity, can effectively support and disperse Co_2B particles, preventing agglomeration and thereby enhancing catalytic reaction activity. To further optimize the catalytic performance, the Fe/Co molar ratio was systematically varied on the same CNTs support. As shown in Fig. 4c and Fig. 4d, the hydrogen evolution rate reached a maximum at a Fe:Co molar ratio of 1:8 and then decreased with increasing cobalt content. This trend suggests that excessive cobalt loading may disrupt the favorable electron redistribution between Co_2B and Fe_2O_3, reducing the overall catalytic efficiency. Additionally, the influence of catalyst loading on $NaBH_4$ hydrolysis was investigated by varying the catalyst amount from 5 to 20 mg (5, 10, 15, and 20 mg) while keeping other reaction parameters constant. As depicted in Fig. 4e and Fig. 4f, the highest hydrogen production rate was achieved with 10 mg of Co_2B/Fe_2O_3-CNTs. This dosage represents the optimal catalyst loading, balancing high activity with cost-effectiveness for practical applications. Meanwhile, the influence of CNTs loading on the hydrolysis of $NaBH_4$ was systematically explored. The hydrogen generation rate was optimized at a CNTs loading of 50 mg, and both insufficient and excessive loadings deteriorated the overall catalytic performance (Fig.S8).

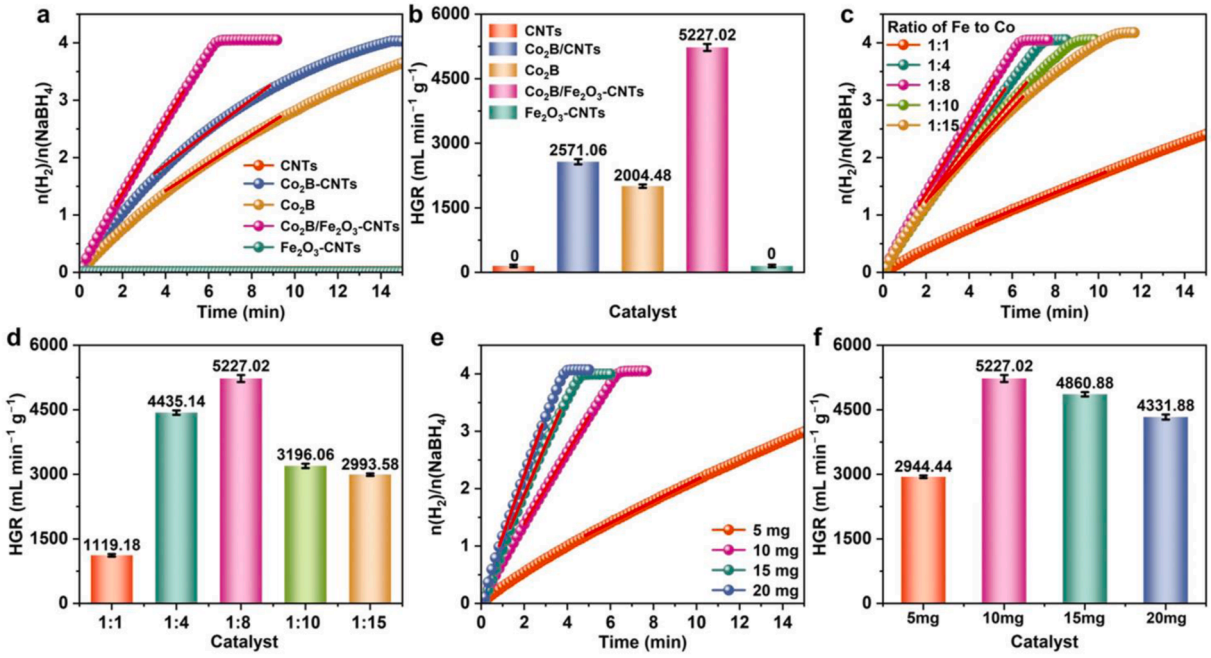

Fig. 4. (a) The equivalent H_2 per mole of sodium borohydride versus time with different catalysts and (b) the corresponding HGR values. (c) Stoichiometric H_2 evolution in 150 mM $NaBH_4$ + 0.4 wt% NaOH solution using Co_2B/Fe_2O_3-CNTs catalysts with different ratios of Fe to Co at 25 °C and (d) the corresponding HGR values. (e) The equivalent H_2 per mole of sodium borohydride versus time with different masses of catalyst and (f) the corresponding HGR values.

To investigate the influence of $NaBH_4$ concentration on catalytic hydrogen production, hydrogen generation rates were evaluated across a range of $NaBH_4$ concentrations while maintaining a constant NaOH concentration. As shown in Fig. 5a, variations in sodium borohydride concentration had a negligible impact on the hydrogen production rate. The inset of Fig. 5a presents the relationship between ln (rate) and ln ($NaBH_4$), yielding a slope of 0.098, which is nearly zero. These findings indicate that the hydrolysis reaction of $NaBH_4$ follows zero-order kinetics with respect to $NaBH_4$ concentration, consistent with previous reports [63]. NaOH is commonly added as a stabilizer in $NaBH_4$ hydrolysis systems to suppress self-hydrolysis. Fig. 5b demonstrates that increasing the NaOH concentration from 0 wt% to 0.8 wt% resulted in minimal changes in the H_2 production rate, confirming the enhanced stability of $NaBH_4$ under alkaline conditions [64]. NaOH of 0.4 wt% was selected as the standard reaction condition because it suppresses spontaneous $NaBH_4$ hydrolysis, ensuring reliable and reproducible catalytic measurements. Additionally, this concentration is widely used in reported $NaBH_4$ hydrolysis studies, enabling fair performance comparison while maintaining stable reaction conditions consistent with common experimental practices. Kinetic measurements were conducted at different temperatures (298, 303, 308, 313, and 318 K) to determine the activation energy (E_a) of the reaction, with fixed concentrations of both the Co_2B/Fe_2O_3-CNTs catalyst and the $NaBH_4$ aqueous solution. As illustrated in Fig. 5c and Fig. S8, the hydrogen evolution rate increased markedly with rising temperature and exhibited a nearly linear dependence on reaction time (Table S1). Based on Arrhenius plot analysis, the activation energies for Co_2B/Fe_2O_3-CNTs and Co_2B were determined to be 52.82 kJ mol^{-1} and 52.36 kJ mol^{-1}, respectively (Fig. 5d). Although the activation energies are similar, catalytic performance may be influenced by multiple factors beyond E_a, including electron density at active sites, multicomponent synergistic effects, and reaction environment. Therefore, direct comparison of catalytic efficiency based solely on activation energy may be insufficient and should be complemented by other kinetic and structural analyses.

To evaluate the reusability of Co_2B/Fe_2O_3-CNTs, cycling stability tests were conducted (Fig. 5e and Fig. 5f). The results show that the HGR gradually decreased over successive cycles, retaining approximately 70% of its initial value by the fifth cycle. Despite this decline, the catalytic activity remained higher than the initial hydrogen production rates of most previously reported catalysts (Table S3). To investigate the underlying causes of the observed activity loss, the Co_2B/Fe_2O_3-CNTs catalyst was systematically characterized after five reaction cycles using XRD, SEM, XPS, and ICP-MS. As shown in Fig. S9, the XRD spectrum indicates that the material retains a similar structural composition after five cycles. SEM images (Fig. S10) show noticeable agglomeration on the catalyst surface after repeated use in $NaBH_4$ hydrolysis, potentially reducing the number of accessible active sites. XPS survey spectra confirm the presence of Co, Fe, and B elements across the entire energy range, consistent with the pre-cycling composition (Fig. S11). High-resolution XPS analyses (Figs. S12a-c) further demonstrate that the elemental identities, chemical states, and peak intensities remain essentially unchanged after five cycles, confirming excellent chemical stability. Additionally, ICP-MS analysis (Table S2) indicates only minor reductions in cobalt and iron content, verifying minimal leaching of metal components. Therefore, the slight decrease in catalytic performance is primarily attributed to two factors: (i) the highly insoluble byproduct $NaBO_2$ deposits on the catalyst surface, partially encapsulating active particles and limiting reactant access [65]; (ii) the minor detachment of metal species due to chemical erosion during repeated reactions [66]. Despite this, the Co_2B/Fe_2O_3-CNTs catalyst demonstrates excellent hydrogen production activity, strong interfacial properties, and effective heterojunction synergy, highlighting its potential for efficient hydrogen generation applications. The catalytic performance of as-prepared Co_2B/Fe_2O_3-CNTs not only surpasses that of Co_2B but also outperforms the majority of catalysts documented in existing literature, as summarized in Fig. 5g and Table S4. Furthermore, as shown in Fig. 5h, the catalyst exhibits excellent magnetic properties, enabling facile magnetic separation and recycling in practical applications. This work demonstrates that regulating the Co_2B/Fe_2O_3 heterojunction interface enhances charge transfer and catalytic performance, offering theoretical insight into structure–charge–activity relationships in non-precious metal catalysts. The catalyst shows strong potential for cost-effective hydrogen production, portable energy systems, and scalable hydrogen technologies, positioning it as a promising alternative to

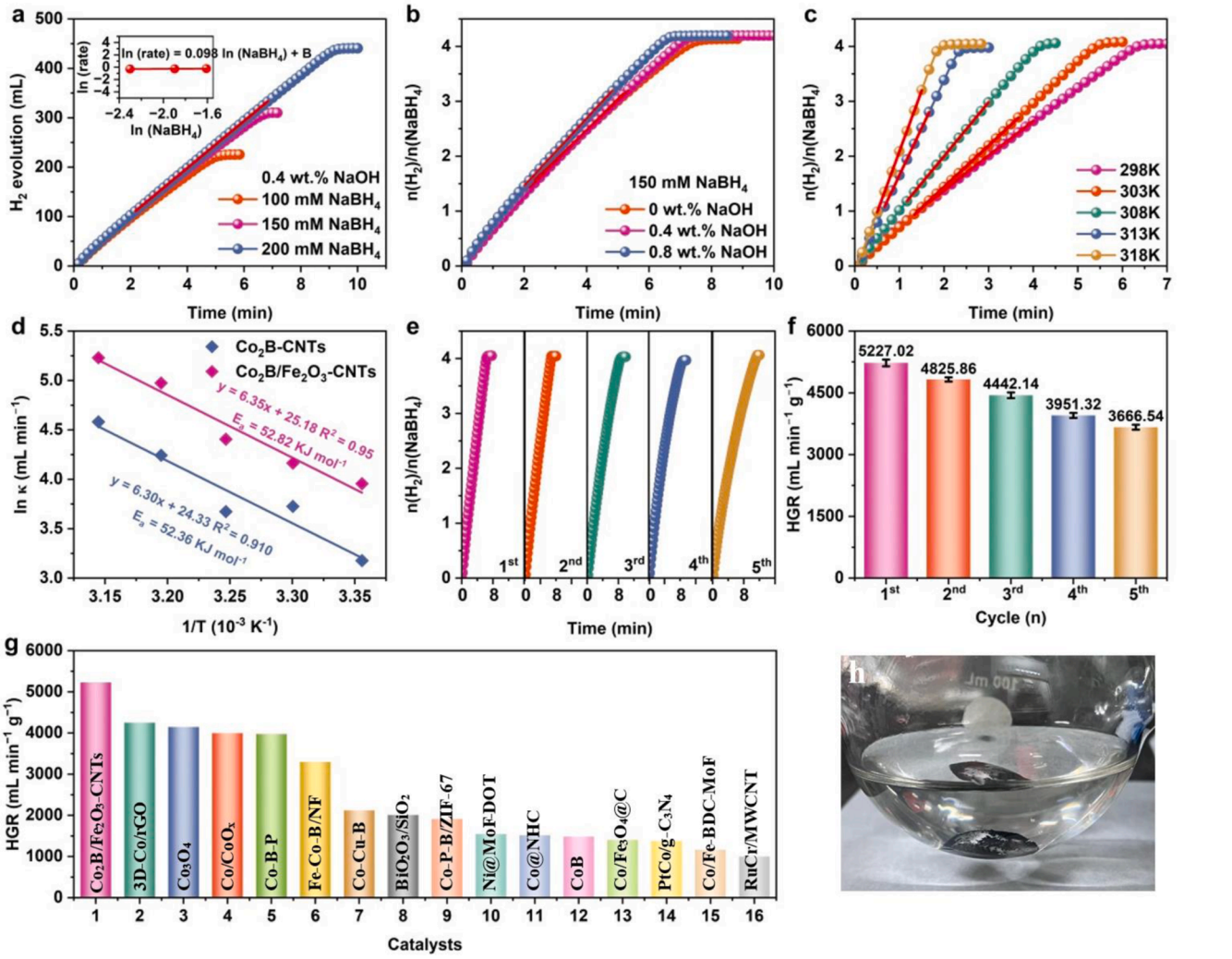

Fig. 5. (a) Effect of different $NaBH_4$ contents on the HGR of the Co_2B/Fe_2O_3-CNTs at a fixed NaOH concentration (0.4 wt%). (b) Effect of different NaOH contents on the HGR of the Co_2B/Fe_2O_3-CNTs at the same $NaBH_4$ concentration (150 mM). (c) Curves of the hydrolysis of alkaline $NaBH_4$ solution at different reaction temperatures in the range of 298–318 K. (d) Arrhenius plots of the different catalysts. (e) Reusability test of the Co_2B/Fe_2O_3-CNTs catalyst in alkaline $NaBH_4$ solution at 25 °C and (f) the corresponding HGR values in the different cycles. (g) Comparison of HGR values for different catalysts (Table S4). (h) Magnetic display picture after Co_2B/Fe_2O_3-CNTs catalyst reaction. All tests were performed in 150 mM $NaBH_4$ + 0.4 wt% NaOH solution.

precious-metal catalysts.

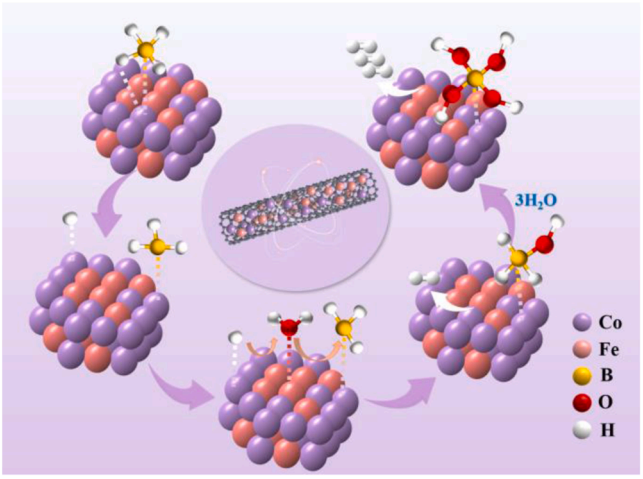

Fig. 6. Proposed mechanism diagram of $NaBH_4$ hydrolysis for H_2 generation.

Based on the above findings, a plausible reaction mechanism is proposed in accordance with the Michaelis-Menten model (Fig. 6). Previous studies have demonstrated that transition metal oxides exhibit a strong affinity for oxygen atoms, enabling water molecules to readily activate lattice oxygen and generate hydroxyl species, thereby promoting efficient cleavage of the HO–H bond [67]. In the Co_2B/Fe_2O_3-CNTs heterostructure, BH_4^- preferentially adsorbs onto Co_2B sites, while H_2O molecules are adsorbed onto Fe_2O_3 sites. The proposed catalytic pathway proceeds as follows: (1) BH_4^- initially adsorbs onto the Co_2B surface; (2) the B–H bond is activated at the Co_2B site, leading to its dissociation into H^- and BH_3; (3) the generated H^- rapidly reacts with protonated H_2O adsorbed on the Fe_2O_3 site, resulting in the release of one H_2 molecule; (4) the remaining OH^- nucleophilic attack the adsorbed BH_3, forming BH_3OH^-, completing the first hydrogen evolution step of $NaBH_4$ hydrolysis; (5) subsequent hydrogen atoms from BH_3OH^- continue to adsorb onto the Co_2B surface; (6) as the reaction progresses, the residual boron-containing intermediates undergo progressive substitution by OH^- ions, ultimately yielding $B(OH)_4^-$ as the final product.

$$BH_4^- \rightleftharpoons BH_3 + H^- \quad (1)$$

$$H^- + H_2O \rightleftharpoons H_2 + OH^- \quad (2)$$

$$OH^- + BH_3 \rightleftharpoons BH_3OH^- \quad (3)$$

$$OH^- + BH(OH)_3^- \rightleftharpoons B(OH)_4^- + H^- \quad (4)$$

4. Conclusion

In summary, we report the successful synthesis of a heterostructure Co_2B/Fe_2O_3 catalyst using CNTs as a support matrix. Comprehensive experimental characterization and catalytic evaluation demonstrate that the optimized Co_2B/Fe_2O_3-CNTs exhibits exceptional catalytic activity in sodium borohydride hydrolysis, achieving a HGR of 5227.02 mL min^{-1} g_{cat}^{-1}, surpassing most reported non-precious metal catalysts. The high performance of this catalyst is attributed to three key factors: (i) the higher charge attraction properties and favorable hydrophilicity endow catalyst with a strong adsorption capacity for negatively charged BH_4^-; (ii) the abundant lattice defects and the unique heterojunction architecture that shortens ion diffusion pathways and enhances mass transport efficiency; and (iii) multicomponent synergistic interactions that modulate the electron density at active sites, promoting reactant adsorption and bond cleavage. Moreover, the effective dispersion of active components facilitated by the CNTs support. These attributes collectively render Co_2B/Fe_2O_3-CNTs a highly promising candidate for hydrogen generation applications, particularly in the context of fuel cell systems. This work provides valuable insights into the rational design of high-efficiency $NaBH_4$ hydrolysis catalysts and offers broader implications for advancing sustainable hydrogen production technologies.

CRediT authorship contribution statement

Tayirjan Taylor Isimjan: Writing – review & editing, Validation. **Xiulin Yang:** Writing – review & editing, Supervision, Funding acquisition. **Shuyi Shang:** Investigation. **Boxuan Lu:** Methodology. **Huaxia Zhou:** Writing – original draft, Data curation, Conceptualization.

Declaration of Competing Interest

The authors declare that they have no known competing financial interests or personal relationships that could have appeared to influence the work reported in this paper.

Acknowledgements

This work has been supported by the Guangxi Science and Technology Projects (GUIKE LT2600640010), the National Natural Science Foundation of China (no. 52363028, 21965005), the Natural Science Foundation of Guangxi Province (2021GXNSFAA076001 and 2018GXNSFAA294077), and the Guangxi Technology Base and Talent Subject (GUIKE AD23023004 and GUIKE AD20297039).

Appendix A. Supporting information

Supplementary data associated with this article can be found in the online version at doi:10.1016/j.colsurfa.2026.140411.

Data availability

Data will be made available on request.

References

[1] A. Magnuson, F. Mamedov, J. Messinger, Toward Sustainable H_2 Production: Linking Hydrogenase with Photosynthesis, Joule 4 (2020) 1157–1159.
[2] S. Özkar, M. Zahmakıran, Hydrogen generation from hydrolysis of sodium borohydride using Ru(0) nanoclusters as catalyst, J. Alloy. Compd. 404-406 (2005) 728–731.
[3] J. Liao, Y. Feng, X. Zhang, L. Huang, S. Huang, M. Liu, Q. Liu, H. Li, CuO-Co_3O_4 Composite Nanoplatelets for Hydrolyzing Ammonia Borane, ACS Appl. Nano Mater. 4 (2021) 7640–7649.
[4] H. Li, P. Wen, Q. Li, C. Dun, J. Xing, C. Lu, S. Adhikari, L. Jiang, D.L. Carroll, S. M. Geyer, Earth-Abundant Iron Diboride (FeB_2) Nanoparticles as Highly Active Bifunctional Electrocatalysts for Overall Water Splitting, Adv. Energy Mater. 13 (2023) 2300489.
[5] H. Wang, F. Xu, L. Sun, J. Wu, G. Zhang, Y. Zhu, Q. Shao, Y. Luo, X. Peng, Y. Wang, Y. Gao, Y. Zou, Novel MOF/COF dual carrier anchoring Ru nanoparticles for improved hydrogen production by hydrolysis of $NaBH_4$, J. Alloy. Compd. 978 (2024) 173415.
[6] R.N.E. Tiri, F. Gulbagca, A. Aygun, A. Cherif, F. Sen, Biosynthesis of Ag–Pt bimetallic nanoparticles using propolis extract: Antibacterial effects and catalytic activity on $NaBH_4$ hydrolysis, Environ. Res. 206 (2022) 112622.
[7] X. Liu, W. Sun, J. Chen, Z. Wen, Controllable Electrochemical Liberation of Hydrogen from Sodium Borohydride, Angew. Chem. Int. Ed. 63 (2024) e202317313.
[8] F. Pan, B. Li, E. Sarnello, Y. Fei, X. Feng, Y. Gang, X. Xiang, L. Fang, T. Li, Y.H. Hu, G. Wang, Y. Li, Pore-Edge Tailoring of Single-Atom Iron–Nitrogen Sites on Graphene for Enhanced CO_2 Reduction, ACS Catal. 10 (2020) 10803–10811.
[9] R. Sun, X. Huang, J. Jiang, W. Xu, S. Zhou, Y. Wei, M. Li, Y. Chen, S. Han, Recent advances in cobalt-based catalysts for efficient electrochemical hydrogen evolution: a review, Dalton Trans. 51 (2022) 15205–15226.
[10] J. Wang, D. Ke, Y. Li, H. Zhang, C. Wang, X. Zhao, Y. Yuan, S. Han, Efficient hydrolysis of alkaline sodium borohydride catalyzed by cobalt nanoparticles supported on three–dimensional graphene oxide, Mater. Res. Bull. 95 (2017) 204–210.
[11] A.F. Baye, M.W. Abebe, R. Appiah-Ntiamoah, H. Kim, Engineered iron-carbon-cobalt (Fe_3O_4@C-Co) core-shell composite with synergistic catalytic properties towards hydrogen generation via $NaBH_4$ hydrolysis, J. Colloid Interface Sci. 543 (2019) 273–284.
[12] B. Chen, S. Chen, H.A. Bandal, R. Appiah-Ntiamoah, A.R. Jadhav, H. Kim, Cobalt nanoparticles supported on magnetic core-shell structured carbon as a highly efficient catalyst for hydrogen generation from $NaBH_4$ hydrolysis, Int. J. Hydrog. Energy 43 (2018) 9296–9306.
[13] H. Shi, Q. Li, T. Su, X. Luo, Z. Qin, H. Ji, $CoZn_yB/Nb_2CT_x$(MXene) for cinnamaldehyde hydrogenation to cinnamyl alcohol: Effects of Zn, Appl. Catal. A Gen. 689 (2025) 120024.
[14] H.-B. Dai, Y. Liang, P. Wang, H.-M. Cheng, Amorphous cobalt–boron/nickel foam as an effective catalyst for hydrogen generation from alkaline sodium borohydride solution, J. Power Sources 177 (2008) 17–23.
[15] K. Narasimharao, B.M. Abu-Zied, S.Y. Alfaifi, Cobalt oxide supported multi wall carbon nanotube catalysts for hydrogen production via sodium borohydride hydrolysis, Int. J. Hydrog. Energy 46 (2021) 6404–6418.
[16] F. Mirshafiee, M. Rezaei, Co/Fe_3O_4@GO catalyst for one-step hydrogen generation from hydrolysis of $NaBH_4$: Optimization and kinetic study, Int. J. Hydrog. Energy 48 (2023) 32356–32370.
[17] M.A.R. López, H.V. Fajardo, G.M.D. Ferreira, T.F. de Souza, V.N. Park, A.F.S. Md Santos, T.S. Rodrigues, L.D. Ramos, G.M.D. Ferreira, Biochar-Based Catalyst Derived from Corn Husk Waste for Efficient Hydrogen Generation via $NaBH_4$ Hydrolysis, Waste Biomass-.-. Valoriz. 16 (2025) 4137–4157.
[18] H. Li, Z. Yao, X. Wang, Y. Zhu, Y. Chen, Review on Hydrogen Production from Catalytic Ammonia Borane Methanolysis: Advances and Perspectives, Energy & Fuels 36 (2022) 11745–11759.
[19] Y. Jiang, T. Wang, Y. Zhou, S. Rao, Y. Li, G. Zhou, X. Tang, Y. Guan, Q. Wang, C. Tang, Q. Li, S. Jia, L. Zhang, J. Yin, J. Yang, Polydopamine-enabled photothermal enhancement of CoFeAl layered double hydroxides for sustainable hydrogen production from sodium borohydride, Int. J. Hydrog. Energy 118 (2025) 58–67.
[20] X. Song, S. Wang, F. Wang, Y. Liu, Z. Zuo, S. luo, D. Chen, F. Zhao, Machine learning-assisted catalyst synthesis and hydrogen production via catalytic hydrolysis of sodium borohydride, Int. J. Hydrog. Energy 129 (2025) 130–149.
[21] Y. Wang, F. Xu, W. Liu, Y. Han, X. Yang, K. Zhang, Z. Cao, Y. Wang, S. Wu, G. Li, Preparation of Co-Mn-B/g-C_3N_4/Ni foam catalyst and its catalytic performance for hydrogen generation from the hydrolysis of sodium borohydride solution, Fuel 406 (2026) 136954.
[22] C. Saka, Utilisation of Cu_2O/CuO@N, O doped catalysts on activated carbon particles derived from biological wastes for highly active hydrogen production with sodium borohydride methanolysis, Fuel 388 (2025) 134485.
[23] H. Li, X. Hu, L. Wang, L. Shi, T.T. Isimjan, X. Yang, Kinetically promoted hydrogen generation by Ru nanoparticles decorated CoB_2O_4 on mesoporous carbon spheres with rich oxygen vacancies for $NaBH_4$ hydrolysis, Chem. Eng. J. 481 (2024) 148547.
[24] C. Zhang, L. Wang, C.-D. Wu, Stabilization of transition metal heterojunctions inside porous materials for high-performance catalysis, Dalton Trans. 52 (2023) 8834–8849.
[25] S.-M. Lam, S.-M. Wong, J.-C. Sin, H. Zeng, H. Li, L. Huang, H. Lin, A.R. Mohamed, J.-W. Lim, Z. Qin, Bi-functional $NiFe_2O_4/SrTiO_3$ S-scheme heterojunction for eminent performance photocatalytic treatment of sewage effluent and electrochemical hydrazine determination, Environ. Res. 261 (2024) 119718.
[26] J. Liao, Y. Shao, Y. Feng, J. Zhang, C. Song, W. Zeng, J. Tang, H. Dong, Q. Liu, H. Li, Interfacial charge transfer induced dual-active-sites of heterostructured

$Cu_{0.8}Ni_{0.2}WO_4$ nanoparticles in ammonia borane methanolysis for fast hydrogen production, Appl. Catal. B Environ. 320 (2023) 121973.
[27] Y. Feng, J. Tian, Y. Shao, X. Dyosiba, J. Ren, J. Xiong, Q. Gao, H. Li, Synergistic VO and VN dual vacancies in homometallic Co_3O_4/CoN heterojunction boosting built-in electric field for efficient hydrogen production, Chem. Eng. J. 529 (2026) 172454.
[28] F. Liu, Z. Fan, Defect engineering of two-dimensional materials for advanced energy conversion and storage, Chem. Soc. Rev. 52 (2023) 1723–1772.
[29] L. Shi, K. Zhu, Y. Yang, Q. Liang, Q. Peng, S. Zhou, T.T. Isimjan, X. Yang, Phytic acid-derivative Co_2B-$CoPO_x$ coralloidal structure with delicate boron vacancy for enhanced hydrogen generation from sodium borohydride, Chin. Chem. Lett. 35 (2024) 109222.
[30] L. Shi, K. Zhu, Y. Yang, Y. Liu, S. Xu, T.T. Isimjan, X. Yang, Oxygen-vacancy-rich Ru-clusters decorated Co/Ce oxides modifying ZIF-67 nanocubes as a high-efficient catalyst for $NaBH_4$ hydrolysis, Int. J. Hydrog. Energy 47 (2022) 37840–37849.
[31] H. Chen, X. Yang, P. Lv, P. Tian, S. Wan, Q. Liu, Mn-doped FeS with larger lattice spacing as advance anode for sodium ion half/full battery, Chem. Eng. J. 450 (2022) 137960.
[32] X. Luo, Z. Ma, T. Su, X. Xie, Z. Qin, H. Ji, J. Chen, Benzaldehyde Synthesis by the Selective Oxidation of Cinnamaldehyde Catalyzed by Fe_2O_3-modified SBA-15, ChemistrySelect 9 (2024) e202401475.
[33] J. Liu, G. Ning, K. Shi, M. Zheng, Y. Sun, Y. Gao, Y. Zhang, H. Wang, N-doped hollow porous carbon spheres@Co Cu Fe alloy nanospheres as novel non-precious metal electrocatalysts for HER and OER, Int. J. Hydrog. Energy 47 (2022) 5947–5960.
[34] L. He, Y. Cheng, Q. Li, H. Zhao, M. Wang, X. Shi, X. Zou, Y. Wang, Y. Wei, Intermetallic niobium boride toward efficient adsorption and catalysis of polysulfides in Lithium-Sulfur batteries, Chem. Eng. J. 453 (2023) 139566.
[35] L.B. Frechette, C. Dellago, P.L. Geissler, Consequences of Lattice Mismatch for Phase Equilibrium in Heterostructured Solids, Phys. Rev. Lett. 123 (2019) 135701.
[36] S.K. Baek, J.S. Kim, Y.D. Yun, Y.B. Kim, H.K. Cho, Cuprous/Cupric Heterojunction Photocathodes with Optimal Phase Transition Interface via Preferred Orientation and Precise Oxidation, ACS Sustain. Chem. Eng. 6 (2018) 10364–10373.
[37] X. Lei, J. Wang, T. Wang, X. Wang, X. Xie, H. Huang, D. Li, Z. Ao, Toluene decomposition by non-thermal plasma assisted $CoO_x - \gamma$-Al_2O_3: The relative contributions of specific energy input of plasma, Co^{3+} and oxygen vacancy, J. Hazard. Mater. 456 (2023) 131613.
[38] M. Sathiya, J.B. Leriche, E. Salager, D. Gourier, J.M. Tarascon, H. Vezin, Electron paramagnetic resonance imaging for real-time monitoring of Li-ion batteries, Nat. Commun. 6 (2015) 6276.
[39] D. Roy, K. Panigrahi, B.K. Das, U.K. Ghorui, S. Bhattacharjee, M. Samanta, S. Sarkar, K.K. Chattopadhyay, Boron vacancy: a strategy to boost the oxygen reduction reaction of hexagonal boron nitride nanosheet in hBN–MoS_2 heterostructure, Nanoscale Adv. 3 (2021) 4739–4749.
[40] Y. Luo, Y. Xia, H. Zhou, C. Yin, H. Yang, J. Chen, L. Ou, Effect of calcium ions on surface properties of chalcopyrite and arsenopyrite and its response to flotation separation under low-alkalinity conditions, Appl. Surf. Sci. 602 (2022) 154191.
[41] Y. Wu, Y. Chen, D. Li, D. Sajjad, Y. Chen, Y. Sun, S. Liu, J. Shi, Z. Jiang, Interface engineering of organic-inorganic heterojunctions with enhanced charge transfer, Appl. Catal. B Environ. 309 (2022) 121261.
[42] X. Xie, M. Peng, W. Li, L. Ma, Z. Qin, T. Su, X. Luo, J. Chen, Z. Yan, H. Ji, Preparation of rapidly absorbing bagasse cellulose-based composite superabsorbent material with semi-interpenetrating networks and its water absorption mechanism, Int. J. Biol. Macromol. 321 (2025) 146125.
[43] Y. Yang, Y. Huang, S. Zhou, Y. Liu, L. Shi, T.T. Isimjan, X. Yang, Delicate surface vacancies engineering of Ru doped MOF-derived Ni-NiO@C hollow microsphere superstructure to achieve outstanding hydrogen oxidation performance, J. Energy Chem. 72 (2022) 395–404.
[44] F. Pan, Z. Li, Z. Yang, Q. Ma, M. Wang, H. Wang, M. Olszta, G. Wang, Z. Feng, Y. Du, Y. Yang, Porous FeCo Glassy Alloy as Bifunctional Support for High-Performance Zn-Air Battery, Adv. Energy Mater. 11 (2021) 2002204.
[45] T. Tang, Y. Teng, K. Sun, Y. Liu, Z. Gao, T.T. Isimjan, J. Guo, J. Tian, X. Yang, Crystal phase engineering and surface reconstruction in Co–Mn phosphides: unraveling the mechanisms of high-performance water oxidation catalysis, Green. Chem. (2025).
[46] H. Liu, X. Liu, Z. Mao, Z. Zhao, X. Peng, J. Luo, X. Sun, Plasma-activated $Co_3(PO_4)_2$ nanosheet arrays with Co^{3+}-Rich surfaces for overall water splitting, J. Power Sources 400 (2018) 190–197.
[47] Q. Li, H. Shi, T. Su, X. Luo, X. Xie, Z. Qin, H. Ji, Multilayer Nb_2CT_x (MXene) Supports CoB for the Selective Hydrogenation of Cinnamaldehyde to Cinnamyl Alcohol: Effect of the Electron-Modified CoB Site and Lewis Acid Site, Catal. Lett. 154 (2024) 4457–4468.
[48] X. Deng, S. Xia, H. Zhao, J. Wang, Z. Wang, A. Kuklin, H. Ågren, G. Baryshnikov, H. Zhang, A new strategy for boron cluster-based metal boride (Co_2B) synthesis and its applicability to electrocatalytic nitrate reduction, Chem. Eng. J. 485 (2024) 149639.
[49] X. Luo, B. Li, T. Su, X. Xie, Z. Qin, H. Ji, B/g-C_3N_4 for Selectively Regulating Oxygen-Guided Photocatalytic Oxidation of Cinnamaldehyde to Benzaldehyde: Effects of Boron Sources, ACS Catal. 15 (2025) 1097–1111.
[50] H. Zhou, C. Shang, T.T. Isimjan, X. Yang, Amorphous high-entropy Co_3B-HEA: Enhanced $NaBH_4$ hydrolysis catalysis via multi-element synergy, Fuel 416 (2026) 138521.
[51] F. Pan, W. Deng, C. Justiniano, Y. Li, Identification of champion transition metals centers in metal and nitrogen-codoped carbon catalysts for CO_2 reduction, Appl. Catal. B Environ. 226 (2018) 463–472.
[52] F. Pan, H. Zhang, K. Liu, D. Cullen, K. More, M. Wang, Z. Feng, G. Wang, G. Wu, Y. Li, Unveiling Active Sites of CO_2 Reduction on Nitrogen-Coordinated and Atomically Dispersed Iron and Cobalt Catalysts, ACS Catal. 8 (2018) 3116–3122.
[53] J. Ding, Z. Mo, X. Zhu, J. Zhu, R. Yang, R. Li, N. Liu, R. Guo, Amorphous cobalt-iron boride nanoparticles grown on B, N-doped carbon frame for efficient electrocatalytic oxygen evolution, Int. J. Hydrog. Energy 51 (2024) 259–270.
[54] Y. Peng, C. Li, M. Song, Z. Xu, C. Yang, Q. Lu, L. Liu, X. Chen, Y. Liu, J. Yi, Breaking the strength-ductility trade-off in aluminum matrix composite through "dual-metal" heterogeneous structure and interface control, Int. J. Plast. 185 (2025) 104216.
[55] J. Hou, B. Zhang, Z. Li, S. Cao, Y. Sun, Y. Wu, Z. Gao, L. Sun, Vertically Aligned Oxygenated-CoS_2–MoS_2 Heteronanosheet Architecture from Polyoxometalate for Efficient and Stable Overall Water Splitting, ACS Catal. 8 (2018) 4612–4621.
[56] X. Du, J. Huang, J. Zhang, Y. Yan, C. Wu, Y. Hu, C. Yan, T. Lei, W. Chen, C. Fan, J. Xiong, Modulating Electronic Structures of Inorganic Nanomaterials for Efficient Electrocatalytic Water Splitting, Angew. Chem. Int. Ed. 58 (2019) 4484–4502.
[57] Y. Li, J. Liao, Y. Feng, J. Li, Q. Liu, W. Zhou, M. He, H. Li, Built-in Electric Field in Yolk Shell CuO-Co_3O_4@Co_3O_4 with Modulated Interfacial Charge to Facilitate Hydrogen Production from Ammonia Borane Methanolysis Under Visible Light, Adv. Funct. Mater. 34 (2024) 2405361.
[58] F. Pan, B. Li, E. Sarnello, Y. Fei, Y. Gang, X. Xiang, Z. Du, P. Zhang, G. Wang, H. T. Nguyen, T. Li, Y.H. Hu, H.-C. Zhou, Y. Li, Atomically Dispersed Iron–Nitrogen Sites on Hierarchically Mesoporous Carbon Nanotube and Graphene Nanoribbon Networks for CO_2 Reduction, ACS Nano 14 (2020) 5506–5516.
[59] Y. Chen, W. Li, Y. Wang, M. Wang, L. Cheng, L. Sun, P. Yan, Aerogel composite of ultrafine Co_2B supported mesoporous CuCoO and chitosan for catalyzed NaBH4 hydrolysis in hydrogen generation, J. Environ. Chem. Eng. 13 (2025) 118495.
[60] Y. He, Y. Yang, C.R. Bowen, Z. Shu, L. Zheng, N. Tu, T. Lu, W. Li, W. Yang, Double-plasmonic-coupled heterojunction photocatalysts for highly-efficient full-spectrum-light-driven H_2 evolution from ammonia borane, Chem. Eng. J. 481 (2024) 148299.
[61] F. Pan, B. Li, E. Sarnello, S. Hwang, Y. Gang, X. Feng, X. Xiang, N.M. Adli, T. Li, D. Su, G. Wu, G. Wang, Y. Li, Boosting CO_2 reduction on Fe-N-C with sulfur incorporation: Synergistic electronic and structural engineering, Nano Energy 68 (2020) 104384.
[62] G. Huang, L. Zhao, S. Yuan, N. Li, S. Jing, Iron doped mesoporous cobalt phosphide with optimized electronic structure for enhanced hydrogen evolution, Int. J. Hydrog. Energy 47 (2022) 14767–14776.
[63] H. Zhang, L. Zhang, I.A. Rodríguez-Pérez, W. Miao, K. Chen, W. Wang, Y. Li, S. Han, Carbon nanospheres supported bimetallic Pt-Co as an efficient catalyst for $NaBH_4$ hydrolysis, Appl. Surf. Sci. 540 (2021) 148296.
[64] S. Zhou, Q. Yang, Y. Liu, L. Cheng, T. Taylor Isimjan, J. Tian, X. Yang, Electronic metal-support interactions for defect-induced Ru/Co-Sm_2O_3 mesosphere to achieve efficient $NaBH_4$ hydrolysis activity, J. Catal. 433 (2024) 115491.
[65] J. Liao, Y. Li, J. Tian, Y. Feng, Q. Liu, H. Li, Morphology engineering of hollow core@shell structured Co_3O_4@CuO-NiO for fast hydrogen release from ammonia borane methanolysis, J. Colloid Interface Sci. 680 (2025) 78–87.
[66] J. Kirk, Y. Kim, Y.-J. Lee, M. Kim, D.-S. Min, P. Soon Kim, J. Hui Seo, Y. Kim, J. Lee, J. Woo Choung, H. Sohn, S.-W. Nam, C.-W. Yoon, Y. Kim, H. Jeong, Pushing the limits of sodium borohydride hydrolysis for on-board hydrogen generation systems, Chem. Eng. J. 466 (2023) 143233.
[67] H. Gu, J. Lan, Y. Liu, C. Ling, K. Wei, G. Zhan, F. Guo, F. Jia, Z. Ai, L. Zhang, X. Liu, Water Enables Lattice Oxygen Activation of Transition Metal Oxides for Volatile Organic Compound Oxidation, ACS Catal. 12 (2022) 11272–11280.